FRET based ratiometric Ca2+ imaging to investigate immune-mediated neuronal and axonal damage processes in experimental autoimmune encephalomyelitis

ARTICLE *in* JOURNAL OF NEUROSCIENCE METHODS · APRIL 2015

Impact Factor: 2.05 · DOI: 10.1016/j.jneumeth.2015.04.005 · Source: PubMed

8 AUTHORS, INCLUDING:

René Gollan

Johannes Gutenberg-Universität Mainz

9 PUBLICATIONS **9** CITATIONS

SEE PROFILE

Jan Baumgart

Universitätsmedizin der Johannes Gutenbe…

17 PUBLICATIONS **549** CITATIONS

SEE PROFILE

Oliver Griesbeck

Max Planck Institute of Neurobiology

56 PUBLICATIONS **4,197** CITATIONS

SEE PROFILE

Journal of Neuroscience Methods 249 (2015) 8–15

Contents lists available at ScienceDirect

Journal of Neuroscience Methods

journal homepage: www.elsevier.com/locate/jneumeth

Clinical Neuroscience

FRET based ratiometric Ca^{2+} imaging to investigate immune-mediated neuronal and axonal damage processes in experimental autoimmune encephalomyelitis

Volker Siffrin[a,*,1], Jérôme Birkenstock[a], Dirk W. Luchtman[a], René Gollan[a], Jan Baumgart[b], Raluca A. Niesner[c], Oliver Griesbeck[d], Frauke Zipp[a]

[a] Neurology Department, University Medical Center of the Johannes Gutenberg University Mainz, 55131 Mainz, Germany
[b] Central Research Animal Facility, University Medical Center of the Johannes Gutenberg University Mainz, 55131 Mainz, Germany
[c] German Rheumatism Research Center, 10117 Berlin, Germany
[d] Max Planck Institute of Neurobiology, 82152 Martinsried, Germany

HIGHLIGHTS

- We report the use of a genetically encoded FRET-based Ca^{2+} (TN-XXL) sensor for intravital ratiometric Ca^{2+} imaging in the brainstem of living anesthetized mice.
- Intraaxonal free $[Ca^{2+}]$ in axons is increased under inflammatory conditions, representing a sign of axonal dysfunction, and can be monitored by intravital microscopy.
- Immune-neuronal interaction that leads to neuronal $[Ca^{2+}]$ increases in axons/neurons in inflammatory lesions, which is also a sign of neuronal injury.

ARTICLE INFO

Article history:
Received 31 March 2014
Received in revised form 2 April 2015
Accepted 3 April 2015
Available online 10 April 2015

Keywords:
EAE/MS
Two-photon laser scanning microscopy
Intravital microscopy
FRET
Ca^{2+} imaging neurodegeneration

ABSTRACT

Background: Irreversible axonal and neuronal damage are the correlate of disability in patients suffering from multiple sclerosis (MS). A sustained increase of cytoplasmic free $[Ca^{2+}]$ is a common upstream event of many neuronal and axonal damage processes and could represent an early and potentially reversible step.
New method: We propose a method to specifically analyze the neurodegenerative aspects of experimental autoimmune encephalomyelitis by Förster Resonance Energy Transfer (FRET) imaging of neuronal and axonal Ca^{2+} dynamics by two-photon laser scanning microscopy (TPLSM).
Results: Using the genetically encoded Ca^{2+} sensor TN-XXL expressed in neurons and their corresponding axons, we confirm the increase of cytoplasmic free $[Ca^{2+}]$ in axons and neurons of autoimmune inflammatory lesions compared to those in non-inflamed brains. We show that these relative $[Ca^{2+}]$ increases were associated with immune-neuronal interactions.
Comparison with existing methods: In contrast to Ca^{2+}-sensitive dyes the use of a genetically encoded Ca^{2+} sensor allows reliable intraaxonal free $[Ca^{2+}]$ measurements in living anesthetized mice in health and disease. This method detects early axonal damage processes in contrast to e.g. cell/axon morphology analysis, that rather detects late signs of neurodegeneration.
Conclusions: Thus, we describe a method to analyze and monitor early neuronal damage processes in the brain in vivo.

1. Introduction

Multiple sclerosis (MS) has been investigated widely in vitro and in its animal model experimental autoimmune encephalomyelitis. The most effective treatment options in MS stem from animal models and target the inflammatory process. However, there is still a large gap between the efficacy of therapies in the animal model experimental autoimmune encephalomyelitis (EAE) and

* Corresponding author at: Klinik und Poliklinik für Neurologie, Universitätsmedizin Mainz, Johannes-Gutenberg Universität Mainz, Langenbeckstr. 1, 55131 Mainz, Germany. Tel.: +49 30 450 540294; fax: +49 30 450 540908.
E-mail address: siffrinv@gmx.de (V. Siffrin).
[1] Current address: ECRC, Charité Campus Buch, Lindenberger Weg 80, 13125 Berlin, Germany.

http://dx.doi.org/10.1016/j.jneumeth.2015.04.005
0165-0270/

MS. Many of these discrepancies arise from the need for induction of the model disease whereas MS has not so far been shown to have an obvious trigger. EAE, however, needs to be induced by subcutaneous immunization of a myelin peptide in strong pro-inflammatory adjuvants, which explains the overwhelming effectiveness of anti-inflammatory treatment strategies in the model system. In MS, however, the major clinical deficits arise from ongoing neurodegeneration in a rather low-level inflammatory environment. Therefore, it is still debated whether even strong anti-inflammatory treatments are really effective in avoiding long-term disability in MS patients or if there is also an independent neurodegenerative aspect to the disease.

In the live animal, it is difficult to differentiate using standard techniques whether the investigated treatment approach is directed against the mode of induction or is actually effective at the site of inflammation, i.e., in the inflamed CNS. We propose a two-photon-based imaging setup, which allows the damage processes to be monitored within inflammatory lesions in the CNS. A central player in intracellular damage processes, in particular in neurons, is Ca^{2+}. $[Ca^{2+}]$ is strongly regulated in the neuronal compartment as sustained $[Ca^{2+}]$ elevation is sufficient to induce axonal damage and Wallerian degeneration (Schlaepfer and Zimmerman, 1985; George et al., 1995). We have previously shown that sustained $[Ca^{2+}]$ in morphologically damaged axons can lead to axonal damage (Siffrin et al., 2010a). Considering all of these findings, we think that monitoring neuronal $[Ca^{2+}]$ as a central mechanism of damage processes, even early in the damage cascade, is a promising way to investigate the damage processes and to evaluate therapeutic approaches toward neuroprotection or neuroregeneration.

There are different possibilities for measuring $[Ca^{2+}]$ within living cells. On the one hand, there are Ca^{2+}-sensitive dyes (CSD), which have the advantage of high sensitivity but the disadvantage of unspecific cell labeling, compartmentalization and drainage from the cells. This makes these CSD rather unattractive for long-term imaging experiments in living tissues. The second way to measure $[Ca^{2+}]$ is to use genetically encoded Ca^{2+} sensors (GECI), which initially had rather low sensitivity in first generation constructs but have been expertly improved since. B6.*thy1*-TN-XXL mice specifically express the genetically encoded ratiometric calcium sensor TN-XXL in neurons via the *thy1* promoter. Conformational changes within the protein, which are induced by Ca^{2+}, increase Fluorescence Resonance Energy Transfer (FRET) from donor to acceptor and can be visualized by 2-photon laser scanning microscopy (Mank et al., 2008; Geiger et al., 2012). The TN-XXL sensor is superior to other third generation GECIs owing to an apparent Kd (approx. 800 nM relevant for both physiologic and pathologic situations in neurons, an improved brightness (better signal), and a much faster response time to Ca^{2+} (142 ms as compared to more than 500 ms for other GECIs) (Whitaker, 2010).

We show that mice with the genetically encoded Ca^{2+} sensor TN-XXL are useful for the identification of damage processes in the brainstem of EAE affected mice.

2. Methods

2.1. Experimental animals

B6.*thy1*-TN-XXL neuronally express the TN-XXL construct, as originally described by Mank et al. (2008). B6.*thy1*-CerTN-L15 mice express the CerTN-L15 construct as described by Heim et al. (2007). Bone marrow chimeric mice were generated by transfer of bone marrow derived cells from donor B6.tdRFP mice into irradiated (30 Gy) B6.*thy1*-TN-XXL mice. After six weeks of homeostatic engraftment, EAE was induced by subcutaneous immunization of myelin oligodendrocyte glycoprotein (MOG) peptide 35–55 in complete Freund's adjuvant (CFA) and intraperitoneal injection of pertussis toxin on d0 and d2. The animal experiments were approved by the appropriate state committees for animal welfare and were performed in accordance with current guidelines and regulations.

2.2. Excitation setup for TPLSM

We employed dual near-infrared (NIR) and infrared (IR) excitation, i.e., two-photon excitation of the sample at 850 nm by an automatically tunable Ti:Sa laser (Mai Tai HP, Spectra Physics, USA) and 1110 nm by an optical parametric oscillator (OPO) pumped by the Ti:Sa laser. The co-localized excitation beams are coupled into a commercially available scan head (TriMScope I, LaVision Biotec GmbH, Bielefeld, Germany) via routing mirrors. The Ti:Sa beam is coupled into an upright microscope (BX-51WI, Olympus, Hamburg, Germany) through the scan–tube lens combination (SL, TL). A dichroic mirror (DM) reflects the excitation beams toward the objective lens (20×, NA 0.95, Olympus Europe, Hamburg, Germany), which focuses them onto the sample at the same spot. Laser-beam scanning is done using a conventional pair of galvanometer scanners that allow free selection of the position and the size of the field of view. In combination with the motorized microscope z-drive, three-dimensional objects can be visualized. In order to increase the penetration depth within tissue, the detection unit is placed in the vicinity of the sample, so that a maximum detection efficiency of the scattered fluorescence photons is achieved. *xyz*-stacks were typically collected within a scan field of 300 μm × 300 μm at 512 × 512 pixel resolution and a *z*-plane distance of 2 μm at a frequency of 400 or 800 Hz. Applied laser powers ranged from 2 to 6 mW at the specimen surface, which allowed for imaging depths up to 150 μm at low photobleaching and with negligible tissue photodamage. Time-lapse series of *xyz* stacks were acquired over several hours, each 60 s.

2.3. Data analysis

Acquired *z*-stacks were exported as tif files and post-processed by the Volocity® software (PerkinElmer, Germany). Noise reduction was achieved by the software's "medium filter". Ratiometric channels were generated using the "ratio" function, which yields a ratiometric channel and an intensity modulated ratio channel (IMR). The latter was used for further $[Ca^{2+}]$ analysis. False-color images of relative Ca^{2+} concentration were generated with ImageJ (NIH, USA). Statistical and mathematical analysis was carried out with Origin (OriginLab Software, USA). Graphical presentation was performed with GraphPad Prism 6 (GraphPad Software, USA).

3. Results

3.1. Long-term intravital imaging experiments require complex monitoring of vital parameters to reliably measure intravital Ca^{2+} dynamics

The aim of the animal preparation for imaging was to (i) analyze neuronal somata and axons in an area that is reachable by TPLSM and (ii) identify inflammatory foci in the standard model of experimental autoimmune encephalomyelitis. In general, the brainstem of mice is involved in demyelinating disease in mice and humans, and therefore, we chose the dorsal area of the medulla oblongata, which can be easily exposed on an inclined head between the first cervical and the base of the skull bone (Fig. 1a). Mice were anesthetized using 1.5% isoflurane (Abott) in oxygen/nitrous oxide (2:1) with a facemask. Mice were then tracheotomized and continuously respirated with a Harvard Apparatus Advanced Safety Respirator (Hugo Sachs, Germany). The anesthetized animal was transferred

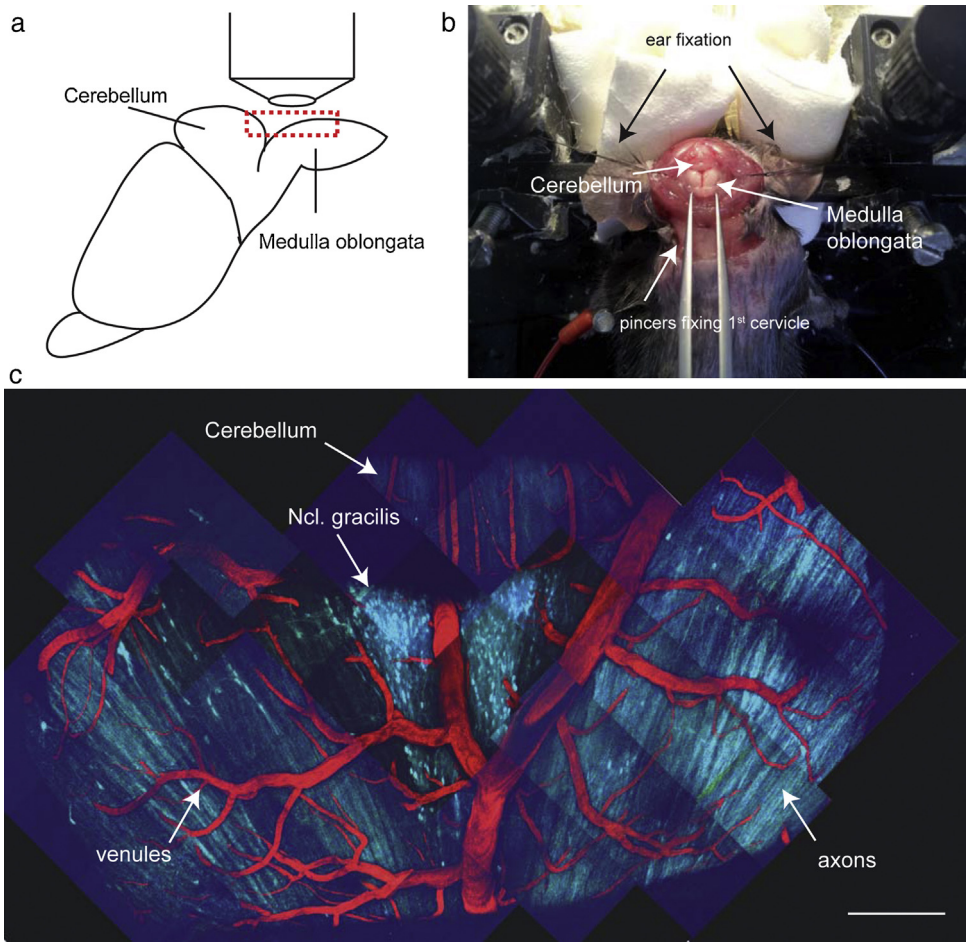

Fig. 1. Intravital imaging of the brainstem of living anesthetized mice. (a) Schematic representation of a mouse brain (sagittal view) illustrates the area of microscopy, which comprises the medulla oblongata, the caudal part of the cerebellum and the upper spinal cord. This imaging area is confined in the *x*–*y* direction by the first cervical and the skull bone. The *z* direction is limited by the maximal penetration depth (ca. 150 μm). (B) Animal preparation of the living anesthetized mouse with exposed brainstem. (C) Two-photon laser scanning microscopy of imaging areas of 300 × 300 × 70–140 μm (*xyz*). Neighboring regions have been scanned consecutively and image stacks have been combined to a photomosaic to give an overview of the microanatomical structures (scale bar: 300 μm).

to a custom-built microscopy table and fixed in a hanging position. The preparation of the imaging field was performed according to adapted protocols for cortical imaging (Göbel and Helmchen, 2007). In brief, the brainstem was exposed by carefully removing musculature above the dorsal neck area and removing the dura mater between the first cervical vertebra and occipital skull bone. The head was inclined to expose the medulla oblongata and part of the cerebellum (Fig. 1b). The dura mater was removed and a sterile agarose patch (0.5% in 0.9% NaCl solution) was installed on the now exposed brain surface to reduce heartbeat and breathing artifacts.

During surgery and microscopy, body temperature was maintained at 35–37 °C and cardiovascular status was monitored by continuous ECG monitoring. Anesthesia depth was controlled by continuous CO_2 measurements of exhaled gas and recorded with a CI-240 microcapnograph (Columbus Instruments, USA). This technique made possible the long-term imaging of the brainstem area of healthy and EAE affected mice over periods of 5–12 h. We used a long-distance water immersion objective (20×) for the imaging area, which was 300 μm × 300 μm × 70 μm (*xyz*). The imaging penetration in the brainstem was limited to about 150 μm (for red fluorescence, a little deeper; see also Herz et al., 2010). In this part of the brain and upper spinal cord, long fiber tracts as well as a neuronal nuclear area – the nucleus gracilis – can be visualized. A photomosaic of a scan of all potential imaging areas (tiles of 300 μm × 300 μm × 70 μm) is shown to give an overview of the reachable brain areas in this model (Fig. 1c). Two medial sensor nuclear areas (nuclei graciles) are generally identifiable, and in addition, large (myelinated) fiber tracts and the caudal part of the cerebellum.

3.2. Determining [Ca^{2+}] by analysis of FRET-signals in intravital recordings

We used *thy1*-promotor driven expression of the Ca^{2+} sensor TN-XXL (Mank et al., 2008; Geiger et al., 2012), which has been reported to measure free [Ca^{2+}] in a relevant range of 10^{-7} to 10^{-5} M. Extracellular homeostatic free [Ca^{2+}] is about 10^{-3} M, whereas cytoplasmic free [Ca^{2+}] is strongly controlled below 10^{-7} M (Ren et al., 2000). Sustained increases in cytoplasmic free [Ca^{2+}] in the μM range have been shown, e.g., in excitotoxic neuronal cell death (DeCoster et al., 1992), and were also shown to induce cytoskeletal changes (Gitler and Spira, 1998). The Kd of TN-XXL has been reported as 830 nM, which indicates that the linear [Ca^{2+}] detection range of TN-XXL should be extremely well suited to investigations of pathophysiologic conditions, i.e., analysis of neuronal and axonal damage processes.

First, we performed, maximal saturation experiments using ionomycin (10 μM) to confirm the usability of the [Ca^{2+}] sensor and to identify saturation levels (Fig. 2). We used naïve B6.*thy1*-TN-XXL mice. The ionomycin was added to the perfusion that continuously

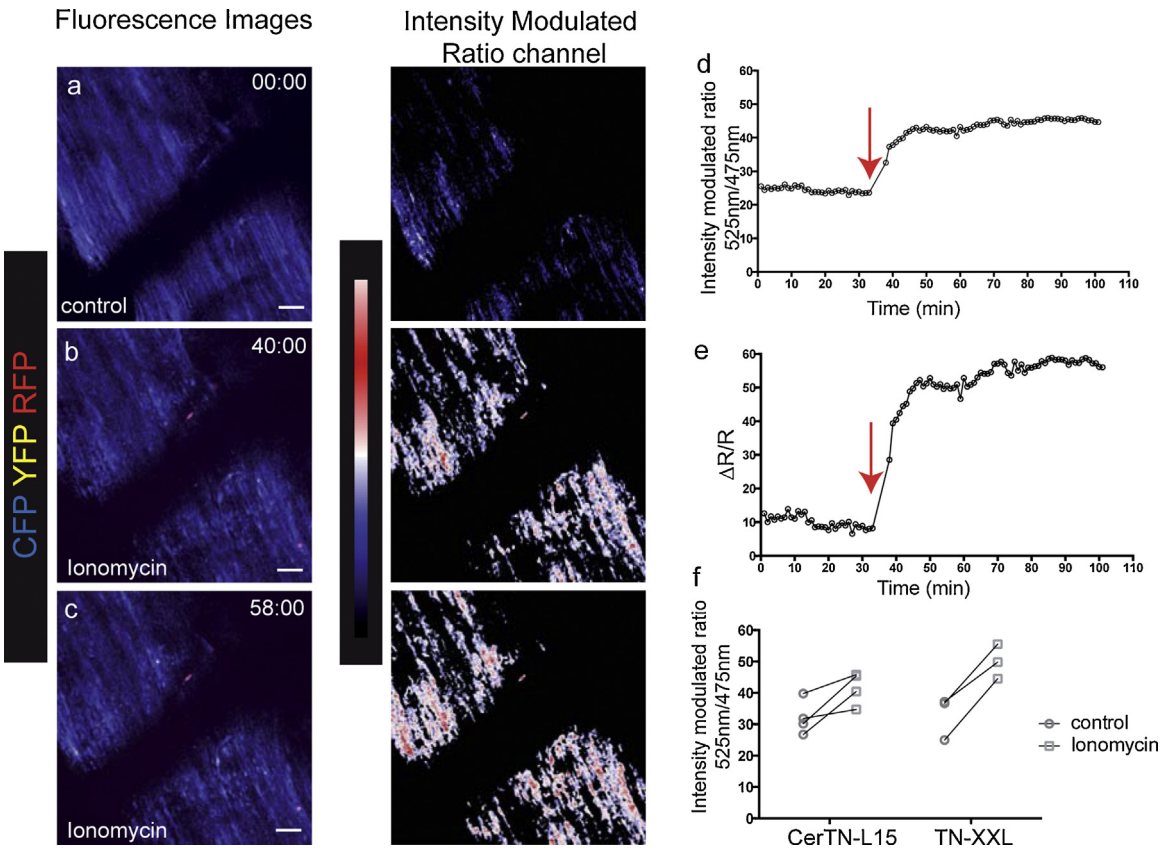

Fig. 2. Intravital imaging of intraaxonal [Ca^{2+}] dynamics in living anesthetized B6.*thy1*-TN-XXL mice. Naïve B6.*thy1*-TN-XXL mice were operated on as described above. TPLSM was performed on the fiber tracts of the medulla oblongata. (a) In the baseline observation time (no compounds added), low fluorescence intensity within axonal structures for CFP and YFP wavelengths and low IMR value were measured (right panel: representation as false color coded image; high IMR value = red, low IMR value = blue, scale bar: 30 μm). (b) After ionomycin (10 μM) was locally applied on the exposed brainstem, IMR color-coded representation revealed strong upregulation of intraaxonal free [Ca^{2+}]. (c) [Ca^{2+}] elevation further progressed over time. (d) Quantification of intraaxonal [Ca^{2+}] levels was performed by identifying axonal structures by CFP fluorescence expression. The sum of signal intensities of the IMR was divided by the volume of the axonal structures (counted as voxels). This mean IMR/axonal volume was presented over the imaging time. The red arrow marks the time point of ionomycin application. (e) Normalization of this IMR/axonal volume (as shown in (d)) was performed using the minimal and maximal IMR signal intensities ($\Delta R/R$) as identified by the histogram function in Volocity®. (f) Comparison of intraaxonal free [Ca^{2+}] in B6.*thy1*-CerTN-L15 and B6.*thy1*-TN-XXL mice in intravital brainstem TPLSM before and after ionomycin application. The mean IMR/axonal volume for 5 consecutive time points before and after application of ionomycin is shown ($n = 4$ for B6.*thy1*-CerTN-L15; $n = 3$ for B6.*thy1*-TN-XXL mice). (For interpretation of the references to color in this figure legend, the reader is referred to the web version of this article.)

exchanges the fluid between the objective lens and brainstem preparation. We have previously reported that with this approach small molecules can efficiently diffuse into the brainstem (Siffrin et al., 2010a). Before adding the ionophore, we recorded a baseline period, which showed low CFP and YFP signals (Fig. 2a, left panel). For analysis of the mean YFP/CFP ratio in the axons or neurons, an intensity modulated ratio channel (IMR) was generated using commercially available software (Volocity®), which was false-color coded (union jack; ImageJ) for visual presentation (Fig. 2a, right panel). Ionomycin application on the living brainstem preparation in the anesthetized mouse induced intraaxonal [Ca^{2+}] changes of the axons in the living anesthetized mice (Fig. 2b), which progressed with time (Fig. 2c). To quantify intraaxonal [Ca^{2+}] and the size/volume of axonal and neuronal structures, we identified axon and neurons using the CFP structure object recognition functionality provided by the Volocity® software (Measurements). The sum of IMR signals for these CFP objects were divided by the whole neuronal volume, resulting in a value per time point (Fig. 2d), which indicates the mean IMR signal intensity per neuronal/axon volume. This was normalized to the minimal and maximal IMR signal intensities ($\Delta R/R$), as identified by the histogram function in Volocity® (Fig. 2e). This showed, as expected, that the mean free [Ca^{2+}] in axons in naïve B6.*thy1*-TN-XXL mice ranges at the lower detection limit of the TN-XXL construct. The dim baseline expression makes the [Ca^{2+}] measurement vulnerable to photobleaching (Fig. 2d). Upon addition of ionomycin, the mean free [Ca^{2+}] increased to the saturation level (Fig. 2d and e).

The TN-XXL construct has improved FRET efficiency and improved dynamic range compared to the CerTN-L15 GECI, which raises the question of the differences in our in vivo application. Therefore, we compared the [Ca^{2+}] response upon ionomycin application in B6.*thy1*-TN-XXL and B6.*thy1*-CerTN-L15 mice, which yielded similar results with a trend toward a broader range of intraaxonal, sustained [Ca^{2+}] levels in B6.*thy1*-TN-XXL mice (Fig. 2f). This underlines the usability of both mouse lines for in vivo brainstem imaging as described here.

Interestingly, the increase of intraaxonal [Ca^{2+}] levels upon ionomycin treatment led to focal morphologic changes, e.g., axonal varicosity/spheroid formation (Fig. 3). These morphologic changes have been associated with a (partially reversible) block of axonal transport and preceding (irreversible) transection (Coleman, 2005).

3.3. Immune cell contacts with axons lead to localized axonal [Ca^{2+}] increases in EAE

To analyze immune-mediated [Ca^{2+}] dynamics in EAE, we generated bone marrow chimeric mice that expressed TN-XXL in

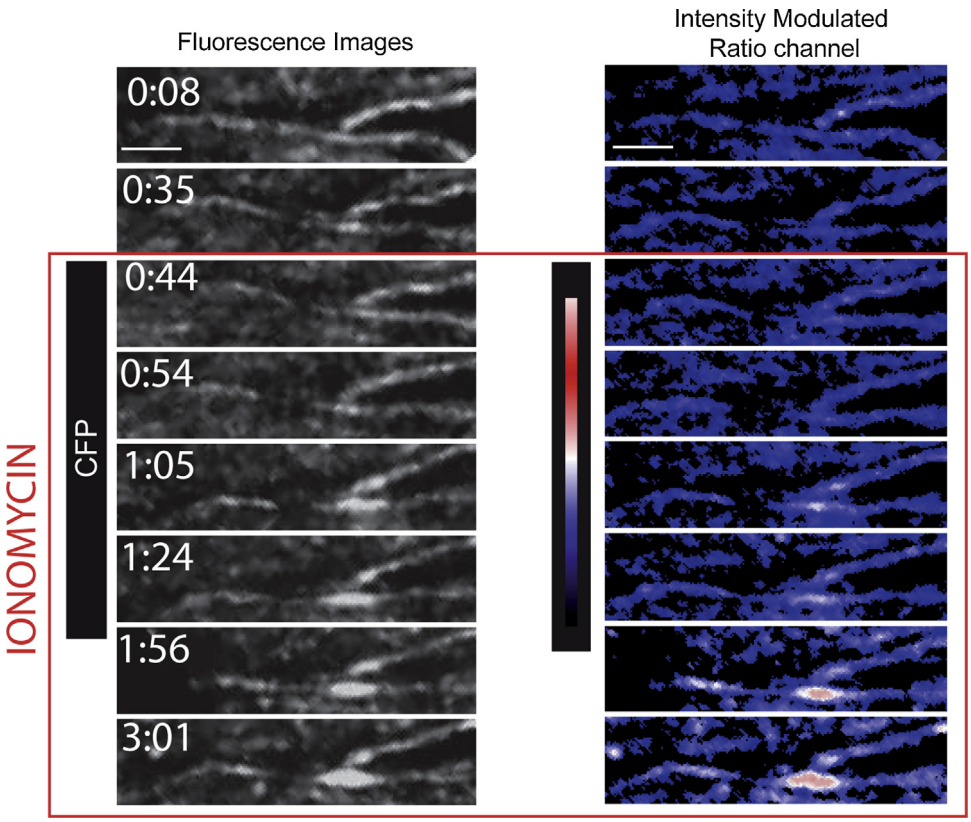

Fig. 3. Long-term TPLSM of intraaxonal free [Ca^{2+}] in B6.thy1-TN-XXL mice after ionomycin. Magnification of single axons in an in vivo preparation similar to that shown in Fig. 2 (scale bar: 20 μm). Time-lapse imaging reveals focal morphologic changes of the axons upon ionomycin treatment. Axonal varicosities and spheroids develop in the areas of raised intraaxonal free [Ca^{2+}].

neurons and axons (B6.*thy1*-TN-XXL) and red fluorescent protein (tdRFP) in hematopoetic cells. EAE was induced in B6.tdRFP->B6.*thy1*-TN-XXL by subcutaneous immunization with $MOG_{35–55}$ and animals underwent microscopy at the peak of the disease. We monitored the [Ca^{2+}] dynamics in fiber tracts of the brainstem (Fig. 4a), which revealed a highly dynamic interaction of the invading immune cells with the axons in vivo. An IMR channel was generated as described in Fig. 2 and is presented as a heat map (see also Siffrin et al., 2010a), which shows that increased [Ca^{2+}] dynamics are often associated with immune cell contacts (Fig. 4b). When IMR/neuronal volume ratio was analyzed as described above and normalized to maximal and minimal values, we clearly identified an overall increase in $\Delta R/R$ in comparison to the non-EAE conditions (Fig. 4c). This increased [Ca^{2+}] of the collectivity of axons was relatively stable over the imaging time of several hours. To further delineate the [Ca^{2+}] dynamics in single axons upon contact with immune cells, we measured single axons using the region of interest function, which allows single axons to be tracked over time. We chose axons with (Fig. 4d) or without sustained immune interactions (Fig. 4e). In addition, the small area of immune-axonal contact was measured separately. To increase the signal-to-noise ratio and to detect potential smaller signal alterations, we normalized these to the overall axonal [Ca^{2+}] ($\Delta R/R_{ROI}/\Delta R/R_{all\ axons}$). The timeline of this normalized $\Delta R/R$ shows that the immune-axonal contact indeed leads to large oscillations of intraaxonal free [Ca^{2+}] (Fig. 4f), which subsides after detachment of immune cells from the axons (which is observable from time point 30 on in the exemplary axon in Fig. 4f and g). This indicates that immune interactions lead to localized [Ca^{2+}] alterations, which are a sign of axonal disturbance/dysfunction.

3.4. Neuronal somata show [Ca^{2+}] increases in EAE as a sign of neuronal injury

Next, we focused on the neuronal somata in the brainstem, which led to the interesting finding of the intense interaction of immune cells with these non-myelinated parts of neurons in demyelinating neuroinflammation (Fig. 5a). These interactions were associated with increased [Ca^{2+}] dynamics as shown by IMR false-color maps (Fig. 5b). We compared different neurons in the preparation before and after ionomycin application to identify the potential of further [Ca^{2+}] increases in these neurons (Fig. 5c and d). Time-lapse imaging revealed that – similarly to the axons – [Ca^{2+}] was increased in certain axons. Neuron 1 showed morphologic signs of cell death, which strongly correlated with a maximal increase in intracellular [Ca^{2+}] elevation that could not be further increased by ionomycin application. Neuron 2 was an example of a dim axon that showed intracellular free [Ca^{2+}] at the lower detection limit (Fig. 5e). Neuron 3 was an example of a neuron with immune interactions that were seen even in the control setting high somatic [Ca^{2+}] with only minor additional increases upon ionomycin application. However, Neuron 3's process, resembling a typical axonal morphology, showed a strong increase in intracytosolic free [Ca^{2+}] (Fig. 5f) and morphologic signs of blebbing. Thus, measurement of intraaxonal free [Ca^{2+}] in EAE preparations can reliably be performed, indicates the early stages of neuronal/axonal

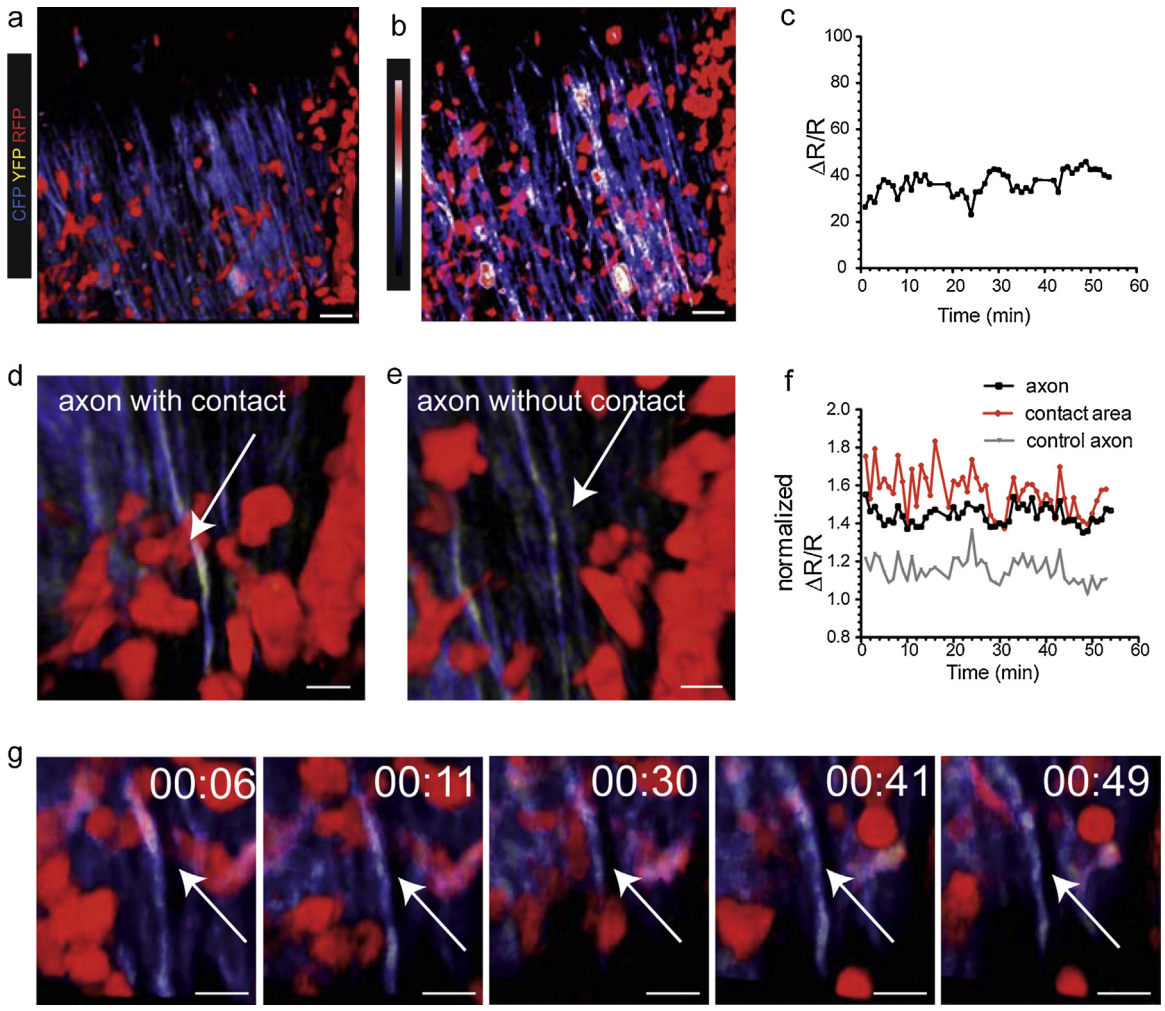

Fig. 4. Intravital imaging of intraaxonal [Ca^{2+}] levels in axons in inflammatory lesion of animals affected by EAE. EAE was in induced in B6.tdRFP->B6.*thy1*-TN-XXL mice by subcutaneous immunization with MOG_{35-55}/CFA. TPLSM in living anesthetized mice was performed at the peak of the disease. (a) Immune cells (RFP, red) infiltrate the axonal area of the brainstem and show close proximity with the axons (TN-XXL = YFP, CFP; yellow, blue; scale bar: 30 μm). (b) False-color-coded representation of the IMR of the same time point as in (a) shows the axonal free [Ca^{2+}] levels in relation to the immune cell proximity. (c) Quantification ($\Delta R/R$) of the whole axonal population over time reveals an increase in intraaxonal free [Ca^{2+}] levels in comparison to naïve mice (see Fig. 2). The raised intraaxonal free [Ca^{2+}] levels are largely stable in the observed time frame. (d) Observation of immune-axonal interaction reveals a localized increased signal intensity in the contacted axon (YFP, CFP; scale bar: 10 μm). (e) Untouched axons exhibit rather low signal intensity (YFP, CFP; scale bar; 10 μm). (f) Quantification of $\Delta R/R_{axon}$, $\Delta R/R_{contact\ area}$ and $\Delta R/R_{control\ axon}$ and representation after normalization with the $\Delta R/R_{all\ axons}$. This reveals that the contacted area shows strong oscillatory free [Ca^{2+}] dynamics upon immune cell interaction, which subsides after immune cell detachment (beyond time point 30). (g) Time-lapse imaging of contacted axon presented in (f); scale bar: 10 μm. (For interpretation of the references to color in this figure legend, the reader is referred to the web version of this article.)

injury and its extreme values also correlate with morphologic signs of axonal and neuronal damage.

4. Discussion

Imaging neuronal and axonal damage in their earliest stages is of great interest for investigations that focus on neuroprotection and neuroregeneration. Live imaging in living anesthetized animals captures the complexity of the whole functioning CNS and reflects the dynamic processes occurring in vivo. We show here that imaging [Ca^{2+}] dynamics in axons and neurons by genetically expressed [Ca^{2+}] sensors is possible in vivo in the brainstem of living anesthetized mice. In addition, we show that intraaxonal and intraneuronal free [Ca^{2+}] are increased during the course of experimental autoimmune encephalomyelitis. It is even possible to monitor single axons and correlate [Ca^{2+}] dynamics to interactions with immune cells. These findings can be exploited to characterize immune-mediated axonal damage processes and to evaluate potential neuroprotective or neuroregenerative therapy regimens.

There has been much debate about how axons and neurons are damaged by autoimmune inflammation in the CNS, and there has been some consensus that the sole removal of the myelin sheath cannot explain the extent of damage to axons in EAE and MS (Trapp et al., 1998; Kuhlmann et al., 2002; Siffrin et al., 2010b). Therefore, the presence of immune cells seems to play an important role, as we and others have shown by live imaging of EAE lesions in the brainstem (Siffrin et al., 2010a) or spinal cord (Nikić et al., 2011). The identification of neuronal and axonal damage processes in vivo is dependent on functional imaging. In this respect, several approaches have been taken to identify axonal and neuronal damage. The most straightforward is to observe axonal morphology, which is, however, a late and rare event in the context of in vivo imaging approaches. Therefore, imaging [Ca^{2+}] dynamics, in particular sustained increases in intracellular [Ca^{2+}], is a promising approach to detect early and potentially reversible axonal injury processes (Siffrin et al., 2010a).

Two-photon laser scanning microscopy is of tremendous value for in vivo imaging studies as they provide high spatial

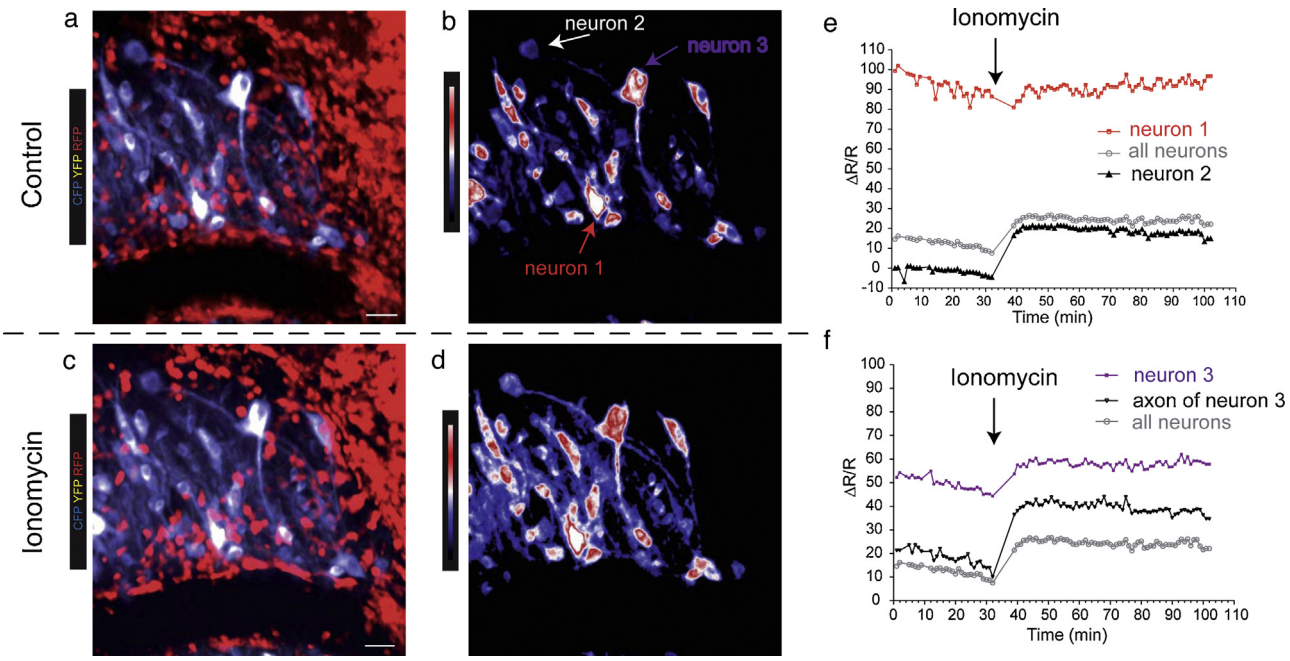

Fig. 5. Intravital imaging of neuronal free [Ca^{2+}] levels in neuronal somata in lesions of EAE affected mice. (a) Immune cells (RFP, red) infiltrate the neuronal nuclear area of the brainstem and show close proximity to the neurons and their processes (TN-XXL = YFP, CFP; yellow, blue). (b) False-color-coded representation of the IMR of the same timepoint as in (a) shows the neuronal free [Ca^{2+}] levels. (c) Ionomycin was added to the preparation as shown in (a). (d) False-color-coded representation of the IMR as shown in (c) shows the increase in free [Ca^{2+}] in the neuronal somata upon ionomcyin application. (e) Quantification ($\Delta R/R$) of distinct neurons as shown in (b). A morphologically shrunken, apopototic neuron (neuron 1) and a low intensity neuron (neuron 2) are shown in relation to $\Delta R/R_{\text{all axons}}$. (f) Quantification of a distinct neuron and its process (neuron 3) is shown in relation to $\Delta R/R_{\text{all axons}}$. (For interpretation of the references to color in this figure legend, the reader is referred to the web version of this article.)

resolutions with penetration depths of several hundred microns in living animals (Herz et al., 2010). In recent years, the development of genetically encoded fluorescent sensors, e.g., the chicken Troponin C based construct TN-XXL, have increased the possibilities of functional imaging. Thereby, genetically encoded calcium indicators (GECI) have important advantages compared to synthetic [Ca^{2+}] sensitive dyes (CSD), e.g., fura-2 or fluo-4, with respect to expression in specific cell populations. In addition, the long-term stability of GECI within the cells is a clear advantage against the dyes that show leakage and compartmentalization (Palmer and Tsien, 2006). Even more important, axons or dendrites can hardly be visualized with CSDs (Looger and Griesbeck, 2012), which makes generation of genetically encoded calcium indicators (GECI) the model of choice for axonal imaging. However, first- and second-generation GECIs, e.g., Calmodulin (CaM)-binding Peptides, had the disadvantage of potential interference with intracellular [Ca^{2+}] dynamics. Therefore, chicken Troponin C based constructs, e.g., TN-L15, represented important progress. These constructs have been successfully applied to in vivo imaging studies. However, compared to the dyes, most of the GECIs had the significant disadvantage of a relatively weak signal intensity and poor intensity range, until recently when diversification and screening of large numbers of sensor variants yielded GECIs that finally exceed the sensitivities of synthetic [Ca^{2+}] dyes in vivo (Thestrup et al., 2014). Furthermore, it could be confirmed that there is no interference with the physiologic function of cells in different systems in the mouse (Mues et al., 2013). Most importantly, GECIs show stable expression in the targeted compartment, which is the main advantage over synthetic dyes, which redistribute and leak continuously after application, interfering with stable experiment conditions in long-term intravital imaging. It has been shown in the context of FRET-based measurements that the apparent dissociation constant Kd of TN-XXL is lower than that of CerTN-L15 due to a stronger involvement of the two high-affinity [Ca^{2+}]-binding sites in TN-XXL. Hence, TN-XXL is able to detect even low but long-lasting [Ca^{2+}] increases in neurons, which indicate early pathology, for instance, in EAE. Moreover, it reacts (binding/unbinding) more quickly to [Ca^{2+}] than CerTN-L15 (311 ms vs. 850 ms/1290 ms) being more sensitive to [Ca^{2+}] concentration changes – however, both GECIs are adequate for pathological cases (long-lasting [Ca^{2+}] increase). The binding sites of TN-XXL are also less sensitive to magnesium, and thus, more specific for calcium.

In the context of in vivo imaging EAE experiments, the main difference between the two GECIs is the FRET efficiency and the resulting dynamic range: TN-XXL has a FRET efficiency twice that of CerTN-L15. This is the most important difference in making TN-XXL more appropriate for in vivo imaging than CerTN-L15, since despite the progress in GECI development, they are still dim in deep tissue due to their blue fluorescing (strongly scattering) donors–variants of CFP. In our preparation and application, we see a trend but no significant superiority of TN-XXL over CerTN-L15, which is most likely due to other factors such as motion artifacts and deep tissue imaging in comparison to ex vivo slice or in vitro cell culture imaging.

Given the intravital imaging conditions, a routine calibration of the mean YFP/CFP ratio as recommended for FRET imaging (Palmer and Tsien, 2006) is not possible. In particular, intact cardiovascular circulation with rapid correction of electrolyte homeostasis interferes with a [Ca^{2+}]-free state. Therefore, special care was taken to ensure that relative changes in the YFP/CFP ratio recorded in our experiments were caused only by changes in the intracellular calcium concentration. While the geometrical factor, bleed-through parameters and direct excitation of the acceptor remain constant over time, they influence only the absolute but not relative values of the YFP/CFP ratio. Since the CFP fluorescence is much more strongly scattered by tissue than Citrine fluorescence, we expect an increased YFP/CFP ratio in deeper layers as compared to the surface. A *z*-drift therefore strongly hampers the comparability of YFP/CFP ratios (data not shown). It should also be taken into account that photobleaching of the fluorescent proteins causes

artifacts in the time course of the mean YFP/CFP ratio. In order to exclude such artifacts, we used low (average and peak) laser powers for excitation, which ensures an overall small amount of photobleaching (Herz et al., 2010). Where necessary, we corrected the time-dependent fluorescence signal of Cerulean and Citrine, respectively, using a monoexponential decay approach for the photobleaching. A solution to overcome these corrections necessary in intravital ratiometric FRET is to employ intravital FRET-FLIM to perform the experiments, as we have shown in a CerTN-L15-based mouse line (Rinnenthal et al., 2013).

In summary, we used the TN-XXL construct for intravital analysis of $[Ca^{2+}]$ dynamics in neurons and axons. Our imaging analysis confirms the sufficient expression of the construct in axons, which is the tremendous advantage over CSD, and neurons for functional $[Ca^{2+}]$ imaging for the identification of intracellular $[Ca^{2+}]$ disturbances, which have been shown to be the initial step in the neurodegeneration process (Siffrin et al., 2010a). Furthermore, we showed that intraaxonal free $[Ca^{2+}]$ was increased in the inflammatory CNS lesions of living anesthetized mice. This could frequently be linked to immune cell contacts and localized peaks of $[Ca^{2+}]$. This shows that there may be several factors that contribute to neuronal and axonal damage processes and might thus be of interest to monitor in EAE lesions. $[Ca^{2+}]$ seems to be an important mediator of sustained damage processes that accurately reflects any kind of damage in the neuronal compartment.

Funding

Gemeinnützige Hertie-Stiftung to VS; German Research Foundation (DFG): SFB-TRR128 to FZ (B4), VS (B9).

References

Coleman M. Axon degeneration mechanisms: commonality amid diversity. Nat Rev Neurosci 2005;6(November (11)):889–98.
DeCoster MA, Koenig ML, Hunter JC, Tortella FC. Calcium dynamics in neurons treated with toxic and non-toxic concentrations of glutamate. Neuroreport 1992;3(September (9)):773–6.
Geiger A, Russo L, Gensch T, Thestrup T, Becker S, Hopfner K-P, et al. Correlating calcium binding, Förster resonance energy transfer, and conformational change in the biosensor TN-XXL. Biophys J 2012;102(May (10)):2401–10.
George EB, Glass JD, Griffin JW. Axotomy-induced axonal degeneration is mediated by calcium influx through ion-specific channels. J Neurosci Off J Soc Neurosci 1995;15(October (10)):6445–52.
Gitler D, Spira ME. Real time imaging of calcium-induced localized proteolytic activity after axotomy and its relation to growth cone formation. Neuron 1998;20(June (6)):1123–35.
Göbel W, Helmchen F. In vivo calcium imaging of neural network function. Physiology (Bethesda, MD) 2007;22(December):358–65.
Heim N, Garaschuk O, Friedrich MW, Mank M, Milos RI, Kovalchuk Y, et al. Improved calcium imaging in transgenic mice expressing a troponin C-based biosensor. Nat Methods 2007;4(February (2)):127–9.
Herz J, Siffrin V, Hauser AE, Brandt AU, Leuenberger T, Radbruch H, et al. Expanding two-photon intravital microscopy to the infrared by means of optical parametric oscillator. Biophys J 2010;98(February (4)):715–23.
Kuhlmann T, Lingfeld G, Bitsch A, Schuchardt J, Brück W. Acute axonal damage in multiple sclerosis is most extensive in early disease stages and decreases over time. Brain J Neurol 2002;125(October (Pt 10)):2202–12.
Looger LL, Griesbeck O. Genetically encoded neural activity indicators. Curr Opin Neurobiol 2012;22(February (1)):18–23.
Mank M, Santos AF, Direnberger S, Mrsic-Flogel TD, Hofer SB, Stein V, et al. A genetically encoded calcium indicator for chronic in vivo two-photon imaging. Nat Methods 2008;5(September (9)):805–11.
Mues M, Bartholomäus I, Thestrup T, Griesbeck O, Wekerle H, Kawakami N, et al. Real-time in vivo analysis of T cell activation in the central nervous system using a genetically encoded calcium indicator. Nat Med 2013;19(June (6)):778–83.
Nikić I, Merkler D, Sorbara C, Brinkoetter M, Kreutzfeldt M, Bareyre FM, et al. A reversible form of axon damage in experimental autoimmune encephalomyelitis and multiple sclerosis. Nat Med 2011;17(April (4)):495–9.
Palmer AE, Tsien RY. Measuring calcium signaling using genetically targetable fluorescent indicators. Nat Protoc 2006;1(3):1057–65.
Ren Y, Ridsdale A, Coderre E, Stys PK. Calcium imaging in live rat optic nerve myelinated axons in vitro using confocal laser microscopy. J Neurosci Methods 2000;102(October (2)):165–76.
Rinnenthal JL, Börnchen C, Radbruch H, Andresen V, Mossakowski A, Siffrin V, et al. Parallelized TCSPC for dynamic intravital fluorescence lifetime imaging: quantifying neuronal dysfunction in neuroinflammation. PLOS ONE 2013;8(4):e60100.
Schlaepfer WW, Zimmerman UJ. Calcium-activated proteolysis of intermediate filaments. Ann N Y Acad Sci 1985;455:552–62.
Siffrin V, Radbruch H, Glumm R, Niesner R, Paterka M, Herz J, et al. In vivo imaging of partially reversible th17 cell-induced neuronal dysfunction in the course of encephalomyelitis. Immunity 2010a;33(September (3)):424–36.
Siffrin V, Vogt J, Radbruch H, Nitsch R, Zipp F. Multiple sclerosis – candidate mechanisms underlying CNS atrophy. Trends Neurosci 2010b;33(April (4)):202–10.
Thestrup T, Litzlbauer J, Bartholomäus I, Mues M, Russo L, Dana H, et al. Optimized ratiometric calcium sensors for functional in vivo imaging of neurons and T lymphocytes. Nat Methods 2014;11(February (2)):175–82.
Trapp BD, Peterson J, Ransohoff RM, Rudick R, Mörk S, Bö L. Axonal transection in the lesions of multiple sclerosis. N Engl J Med 1998;338(January (5)):278–85.
Whitaker M. Genetically encoded probes for measurement of intracellular calcium. Methods Cell Biol 2010;99:153–82.